

# Multilayer SnS Field-effect Transistors and the Critical Role of Carrier Screening in Their Performance-limit

Sukrit Sucharitakul,<sup>†</sup> Rajesh Kumar Ulaganathan,<sup>‡,Δ</sup> Raman Sankar,<sup>§,⊥</sup> Fang-Cheng Chou,<sup>§</sup> Yit-Tsong Chen,<sup>‡,Δ</sup> Chuhan Wang,<sup>¶</sup> Cai He,<sup>¶</sup> Rui He,<sup>¶</sup> and Xuan P. A. Gao<sup>\*,†</sup>

<sup>†</sup> Department of Physics, Case Western Reserve University, 2076 Adelbert Road, Cleveland OH 44106

<sup>‡</sup> Department of Chemistry and <sup>§</sup> Center for Condensed Matter Sciences, National Taiwan University, Taipei 10617, Taiwan

<sup>⊥</sup> Institute of Physics, Academia Sinica, Taipei 11529, Taiwan

<sup>Δ</sup> Institute of Atomic and Molecular Sciences, Academia Sinica, Taipei 10617, Taiwan

<sup>¶</sup> Department of Physics, University of Northern Iowa, Cedar Falls, Iowa 50614, USA

\* Address correspondence to [xuan.gao@case.edu](mailto:xuan.gao@case.edu) (X.P.A.G.)

## ABSTRACT

Gate tunable p-type multilayer tin mono-sulfide (SnS) field-effect transistor (FET) devices with SnS thickness between 50 and 100 nm were fabricated and studied to understand their performances. While reasonable field effect mobilities ( $\sim 5 \text{ cm}^2/\text{Vs}$ ) in the linear regime was obtained, the devices showed finite OFF state conductance and an ON-OFF ratio  $\sim 10$ . The poor gate tuning behavior in the depletion regime of SnS devices studied is attributed to the finite screening length effect of unintentionally doped holes in SnS. Through etching and n-type surface doping by  $\text{Cs}_2\text{CO}_3$  to reduce/compensate the not-gatable holes near SnS flake's top surface, the devices gained an order of magnitude improvement in the ON-OFF ratio and hole Hall mobility  $\sim 100 \text{ cm}^2/\text{Vs}$  at room temperature. This work suggests that in order to obtain effective switching and low OFF state power consumption, two-dimensional (2D) semiconductor

based depletion mode FETs should limit their thickness to within the Debye screening length of carriers in the semiconductor.

KEYWORDS: 2D semiconductor, SnS, tin mono-sulfide, FET, doping, screening, ON-OFF ratio

Since the work by Novoselov and coworkers on exfoliable 2D van der Waals (vdW) materials<sup>1</sup> and studies that demonstrated Dirac electrons in graphene,<sup>1-2</sup> scientists and engineers have been conducting enormous amount of research on the topic. A wide variety of 2D materials were explored and studied for their exotic electrical and optical properties, in particular, transitional metal dichalcogenides (TMDs)<sup>3-7</sup> such as MoS<sub>2</sub><sup>8-10</sup>, MoSe<sub>2</sub><sup>11,12</sup>, WS<sub>2</sub><sup>13,14</sup> and WSe<sub>2</sub><sup>15,16</sup>. In addition to TMDs, the pursuit of 2D semiconductors for high performance electronics or optoelectronics is extended to non-TMDs such as phosphorene<sup>17,18</sup> and III-VI materials (e.g. InSe).<sup>19,20</sup> Among the numerous 2D semiconductors that have been explored, many high quality n-type materials or device structures have been developed. Achieving high performance p-type devices has been more challenging. Notable recent progresses in this area are black phosphorus devices<sup>17, 18</sup> and novel p-type contact scheme for hole injection into TMD devices.<sup>21</sup> Tin monosulfide (SnS), a IV-VI compound semiconductor, is a layered vdW material with Pnma crystal structure. In the past, due to its 1.07 eV band gap and its high optical absorption coefficient above band gap<sup>22,23</sup>, SnS has been mainly studied for solar cell applications.<sup>23</sup> More recently, the electronic and thermal properties of bulk SnS and SnSe have attracted increasing attention for thermoelectric applications.<sup>24-26</sup> So far, transport study on nanoscale SnS and SnSe crystals is very limited.<sup>27</sup> Given that bulk SnS has p-type nature and hole mobility of 90 cm<sup>2</sup>/Vs,<sup>28</sup> SnS appears to be a good candidate for use in p-type 2D nanoelectronic devices. The anisotropic crystal structure of SnS also suggests that the transport properties of SnS could be strongly anisotropic within the 2D plane, similar to black phosphorus.<sup>26</sup> However, there has been no carrier transport or field effect device studies on nanoscale SnS. In this work, nanoflakes were exfoliated from bulk SnS single crystal and p-type SnS FET devices were successfully fabricated and studied. We found that due to the high intrinsic p-type doping and strong carrier screening in as grown SnS, the field effect of gate is not sufficient to tune the carrier transport throughout the whole thickness (ca. 50-100 nm) of the devices and renders poor switching behavior. By means

of surface doping to compensate the intrinsic p-type holes or etching to reduce the sample thickness, higher performance (hole Hall mobility  $\sim 100 \text{ cm}^2/\text{Vs}$  at room temperature) and ON-OFF ratio ( $\sim 100$  at room temperature) was realized. In addition to gaining insight on the role of carrier screening as the limiting factor in the switching performance of 2D semiconductor depletion mode FETs, this work paves a way towards high performance 2D electronic devices based on IV-VI semiconductors and the theoretically envisioned novel valleytronics based on single layer SnS.<sup>29</sup>

## RESULTS AND DISCUSSION

The layered vdW crystal structure of SnS is illustrated in the scheme shown in Figure 1a. The structure is highly anisotropic, both along the direction perpendicular to the 2D layer as well as within the two-atom thick 2D layer. Within the 2D layer, the atoms are arranged in the armchair fashion along the z (or c) direction (as shown in Figure 1a) while the y (or b) direction is the zigzag direction. The x-ray diffraction (XRD) data of the bulk SnS crystal used in this work are shown in Figure 1b, confirming its single crystalline quality. Figure 1c shows Raman spectra from 50 nm and 85 nm SnS flakes. Raman spectrum from each sample shows six well-defined peaks, among which four are  $A_g$  modes and two are  $B_{3g}$  modes. The frequencies of these modes are in excellent agreement with those reported for bulk SnS,<sup>30,31</sup> confirming that our samples are in orthorhombic phase. When exfoliated into small multilayer flakes, SnS samples often appear in a shape near a rectangle. To identify the anisotropic electronic properties of SnS, we distinguish the short and long directions of SnS nanoflake samples as the 'A' and 'B' directions, respectively, as noted in the picture of a representative device in Figure 1d. Electron-beam lithography was used to fabricate four-probe devices in the van der Pauw configuration (Figure 1d). Atomic force microscope (AFM) was used to identify the thickness of SnS flakes studied. An example of the height profile of a 64 nm thick SnS flake imaged by AFM is given in Figure 1e.

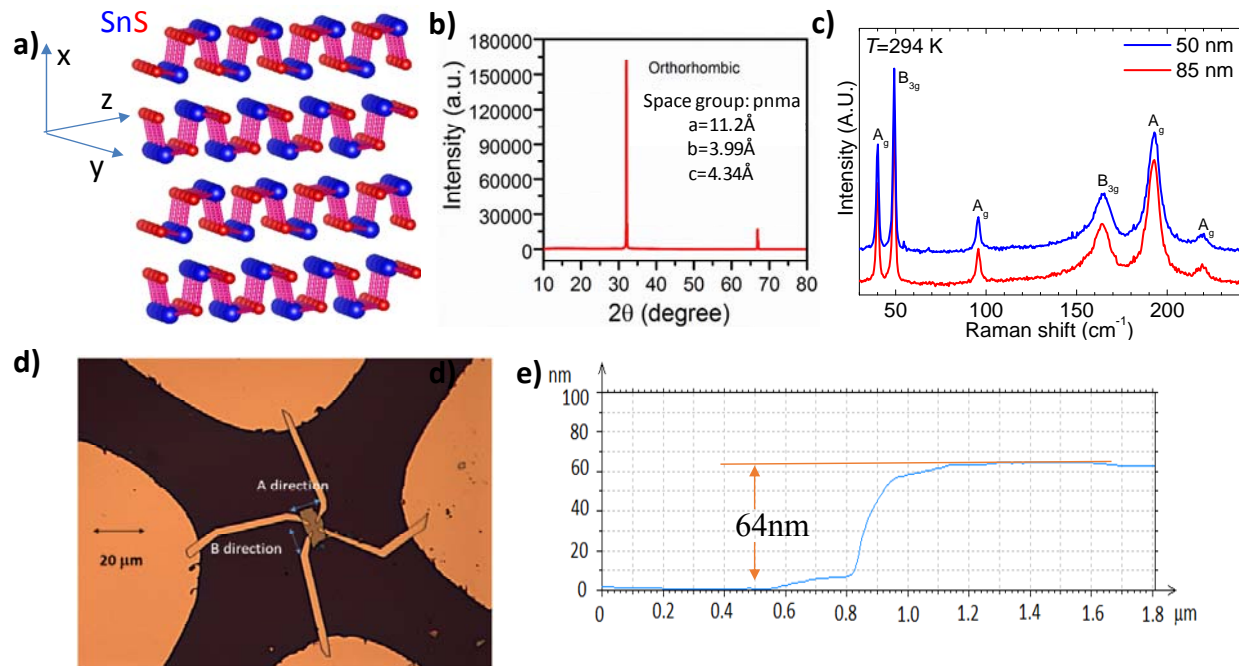


**Figure 1. a) Crystal structure of SnS (Sn in blue and S in red). b) XRD results of a bulk SnS single crystal used. c) Raman spectra from 50 and 85 nm SnS flakes. d) Optical image of a SnS four-probe device. e) AFM height profile of an exfoliated SnS flake used to fabricate device.**

The sample was loaded into a Physical Properties Measurement System (PPMS) for electrical measurements. As demonstrated by the linear relation between the source-drain current  $I_{sd}$  and the source-drain voltage  $V_{sd}$  in Figure 2a, Ohmic contacts were obtained between Ni source/drain contacts and SnS nanoflake. Moreover, the four-probe van der Pauw geometry allowed comparing SnS nanoflake's intrinsic conductance along two orthogonal crystal directions without the influence of contact resistance. Figure 2b presents the four-probe conductance of a SnS nanoflake measured along the A-direction or B-direction as a function of backgate voltage  $V_g$  at  $T=300$  K. The decreasing trend of conductance *vs.*  $V_g$  indicates the p-type nature of the SnS flake. The conductance along the A-direction is generally found to be higher than that measured along B-direction in our van der Pauw devices. For the device in Figure 2b, the conductance ratio between these two directions is about 2.5 (Figure 2b inset). This is consistent with the anisotropic lattice structure and electronic structure in the 2D plane of SnS.<sup>26</sup> It is noteworthy from Figure 2b that the device could not be completely turned off at high positive gate voltages (*i.e.* there is a non-negligible conductance in the OFF state of the device at high  $V_g$ ). Figure 2c further shows

the four-probe conductance  $G$  vs.  $V_g$  along the B direction at different temperatures. The  $G(V_g)$  data at different  $T$  show that raising temperature increases the overall conductance of the device and the device tends to saturate towards a lower OFF state conductance at lower  $T$  as indicated by the dashed horizontal lines in Figures 2c and d. The strong influence of temperature on devices' ON-OFF ratio can be more clearly seen in Figure 2d which displays the  $G(V_g)$  data in semi-log scale. At room temperature, the ON-OFF ratio is  $\sim 10$  and lowering  $T$  to 250 K enhances the ON-OFF ratio to  $\sim 50$ . Figure 2c and d also show noticeable hysteresis effect in the  $G$  vs.  $V_g$  sweep loop, indicating the existence of charge trap states.

From the quasi-linear regime of the  $G(V_g)$  plots at negative  $V_g$ , the field effective mobility  $\mu_{FE}$  can be extracted using the relation  $\mu_{FE} = \frac{g_m}{C_g} / \left(\frac{\pi}{\ln(2)}\right)$ , where  $g_m$  is the trans-conductance or the slope of conductance vs.  $V_g$  while  $C_g$  is the gate capacitance and  $\frac{\pi}{\ln(2)}$  is the correction factor in the van der Pauw method.  $\mu_{FE}$  can be estimated to be around 4-7  $\text{cm}^2/\text{Vs}$  in the temperature range 250 - 350 K. Compared to the  $\sim 90 \text{ cm}^2/\text{Vs}$  hole mobility in bulk SnS, this  $\mu_{FE}$  is about an order of magnitude smaller. Our gate dependent carrier density measurement from the Hall effect showed that the gate capacitance is significantly over-estimated (by about ten times) in the parallel plate capacitance model, due to the disregard of trap states capacitance. Thus this apparent  $\mu_{FE} \sim 4-7 \text{ cm}^2/\text{Vs}$  significantly under-estimates the hole mobility in multilayer SnS.

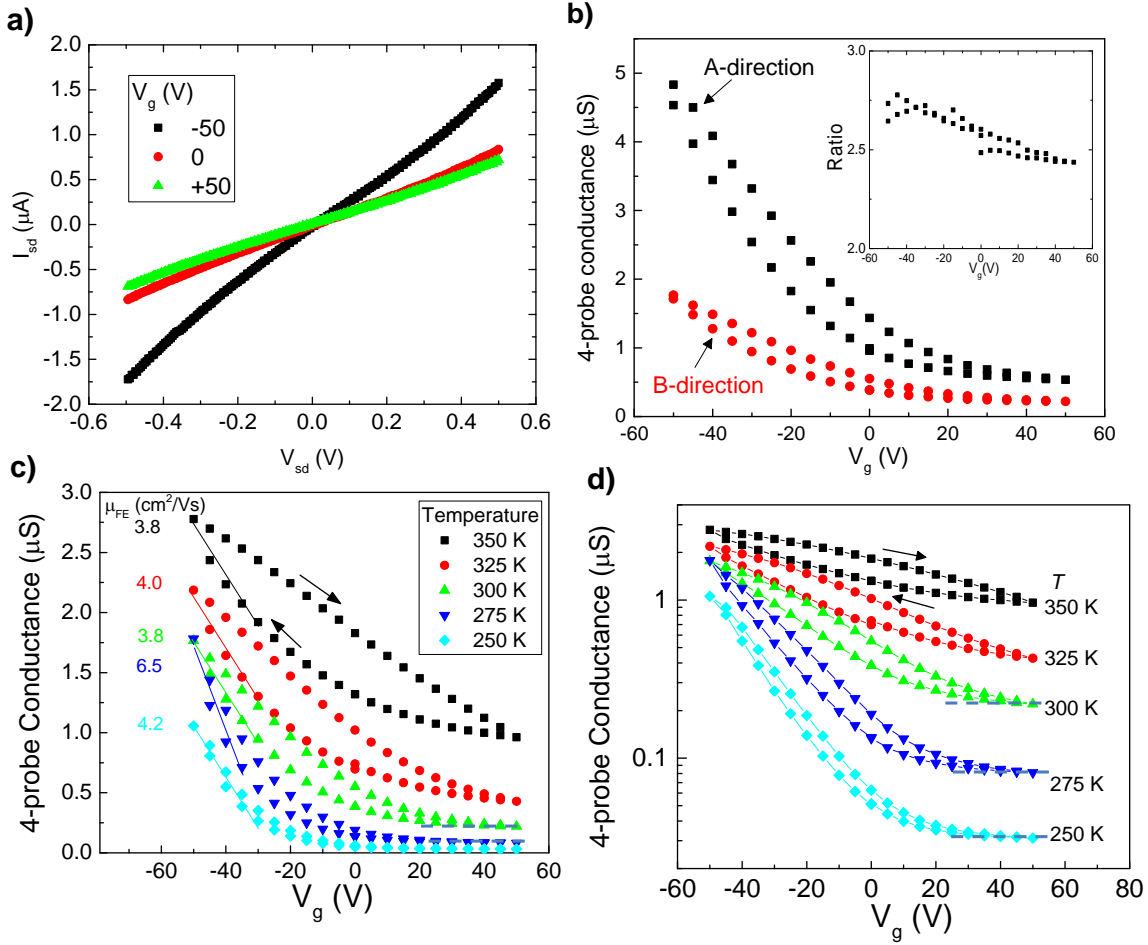


**Figure 2.** a)  $I_{sd}$ - $V_{sd}$  plot of a 60 nm thick multilayer SnS device at 300 K. b) Four-probe conductance vs.  $V_g$  along two perpendicular directions in the 2D plane at 300 K (inset: conductance ratio between the two directions). c) Four-probe conductance vs.  $V_g$  at different temperatures and d) Data in c) shown in semi-log scale.

The behavior of gate being able to enhance the carriers but incapable of depleting carriers in SnS was observed in many devices with thickness in the range of 50 to 100 nm. This characteristics was also quite common in other semiconductor nanoscale FET devices with similar thickness, (e.g. InAs nanowire FETs<sup>32</sup>) and poses a limitation on the performance of semiconductor nanoelectronics. In the following, we will show that this phenomenon is originated from the simple fact that carrier screening length  $L_D$  in semiconductors is finite such that semiconductor FETs with body thickness larger than  $L_D$  has a surface 'dead layer' whose carrier conduction cannot be tuned by the gate.

To comprehend the origin of carriers and the underlying gate tuning mechanism of the transport properties of the device, Hall measurements at different temperatures and back-gate voltages were conducted by the application of perpendicular magnetic field. By measuring the Hall resistance  $R_{xy}$  at various magnetic field  $B$ , we observed a linear relation in  $R_{xy}$  vs.  $B$  and the Hall coefficient can be calculated from  $R_H = \frac{R_{xy}}{B}$ . The hole carrier density can be extracted through relation  $p = \frac{1}{eR_H}$  with  $e$  being the fundamental electron charge. From the hole carrier density  $p$  data shown in Figure 3a, we see that  $p$  increases linearly as  $V_g$  reduces towards the negative direction but it saturates towards a residual value at high positive  $V_g$ , in a similar way to the  $G(V_g)$  data in Figure 2. This suggests that there is a limit on the number of holes that can be removed by applying positive  $V_g$  in these SnS flakes. Moreover, for a given  $V_g$ , there are more carriers at higher temperature, suggesting the thermally excited behavior of carriers. Figure 3b shows the temperature dependence of hole density in the Arrhenius plot. The plot highlights that available hole carrier concentration for electrical transport follows  $p(T) \propto \exp\left(-\frac{\Delta E}{k_B T}\right)$ . Similar thermally activated behavior is seen in the Arrhenius plot for the temperature dependent conductance in Figure 3c. The activation energy  $\Delta E$  extracted from fitting the Arrhenius plots of  $p(T)$  and  $G(T)$  along both the A and B-directions of the SnS flake are displayed in Figure 3d. We see a good agreement between  $\Delta E$  fitted from the thermal activation model for the carrier density and conductance data: the activation energy increases with the gate voltage in the negative  $V_g$  regime and stays relatively constant in the positive  $V_g$  regime. This trend is again correlated with the gate dependent conductance and hole density in Figure 2 and Figure 3a.

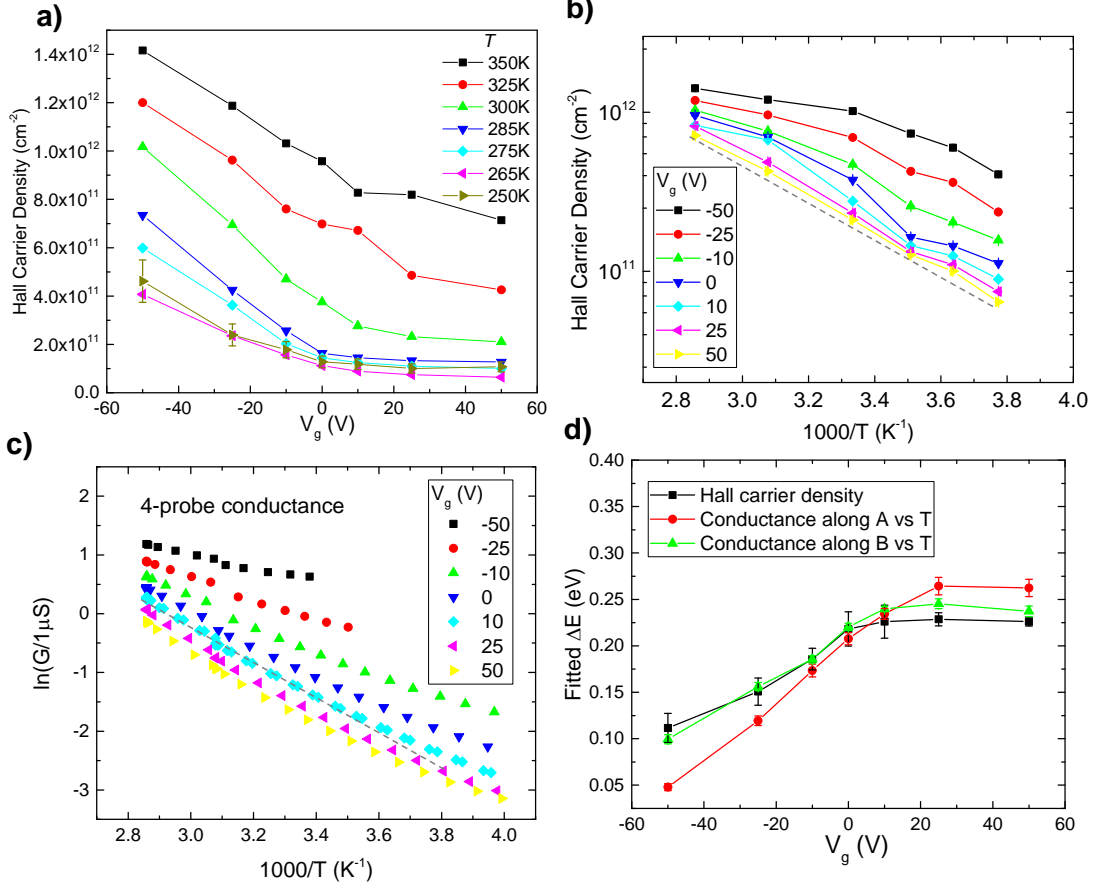


**Figure 3. a) Hall carrier density at different applied backgate voltages. b) Arrhenius plot of Hall carrier density for holes vs.  $1/T$ . c) Arrhenius plot of the four-probe conductance vs.  $1/T$ . d) Fitted activation energy from the temperature dependence of the hole density extracted from the Hall effect or the conductance along the 'A-direction' or 'B-direction' of SnS flake, plotted against the backgate voltage.**

The gate tuned thermally activated transport and the behavior of residual conductance in the high  $V_g$  regime in these SnS devices can be naturally explained by a simple model in which the holes originate from acceptors with ionization energy  $E_a \sim 0.22$  eV (Figure 4a) and the carrier screening effect in semiconductor with thickness exceeding the carrier screening length (Figure 4b). Our estimate of acceptor ionization energy  $\sim 0.22$  eV is based on the activation energy for the carrier density and conductance at  $V_g=0$  in Figure 3d. In the negative gate bias regime, more holes are induced into the bottom surface of SnS flake. This accumulation of holes enhances the conductivity of a layer near the bottom of the flake (with thickness approximately the screening length of carriers) and the measured conductance is dominated by this bottom layer in which the

Fermi energy  $E_F$  is shifted closer to the valence band. Thus a reduced activation energy and increased conductance were observed. On the other hand, when a positive  $V_g$  is applied to deplete the carriers, holes near the bottom surface are first depleted and the conductance of the sample gradually becomes dominated by the holes near top surface where  $p$  and  $E_F$  remain constant. Therefore, the activation energy  $\Delta E$  appears to be pinned at  $\sim 0.22\text{eV}$  by the carriers in the top surface layer.

We next discuss the OFF state performance of depletion mode FET devices made from 2D semiconductors with appreciable thickness and doping, using the multilayer SnS devices in this work as an example. With small  $V_g$ , the depth of bottom surface tuned by gate is approximately the Debye screening length  $L_D = \sqrt{\epsilon k_B T / e^2 p}$  with  $\epsilon$ ,  $k_B$  as the dielectric constant of semiconductor and the Boltzmann constant (Figure 4b). In very high  $V_g$  towards depletion, one reaches the maximum depletion depth when  $E_F$  of bottom surface is tuned to the middle of the bandgap at which point the depletion thickness  $W_D \approx \sqrt{2\epsilon k_B T \ln(N_a / p_i) / e^2 N_a}$  with  $p_i$  and  $N_a$  as the intrinsic carrier concentration and acceptor density.<sup>33</sup> Based on the hole density at  $V_g=0$ , we estimate the acceptor doping level  $N_a$  to be greater than  $10^{18}/\text{cm}^3$  in our SnS. This leads to a maximum depletion width  $W_D$  to be a few tens of nm or less at 300K.<sup>33</sup> Therefore, when a large gate voltage is used to deplete carriers in doped 2D semiconductors with thickness  $h > W_D$ , the conduction through the sample is shunted by a 'dead-layer' near the top surface and the device remains to be conductive in the OFF state. The thickness of this 'dead-layer' is approximately  $h - W_D$  and the residual OFF-state conductance in the depletion regime can be

$$G_{\text{OFF}} \approx p e \mu_h W (h - W_D) / L, \quad (1)$$

where  $L$  and  $W$  are the length and width of the sample and  $\mu_h$  is the hole (or majority carrier) mobility. Based on these discussions and the relatively large thickness of SnS employed here (50-100 nm), we see that the poor gate tuning performance in the positive gate voltage regime is caused by the shunt effect from holes in the surface dead-layer.

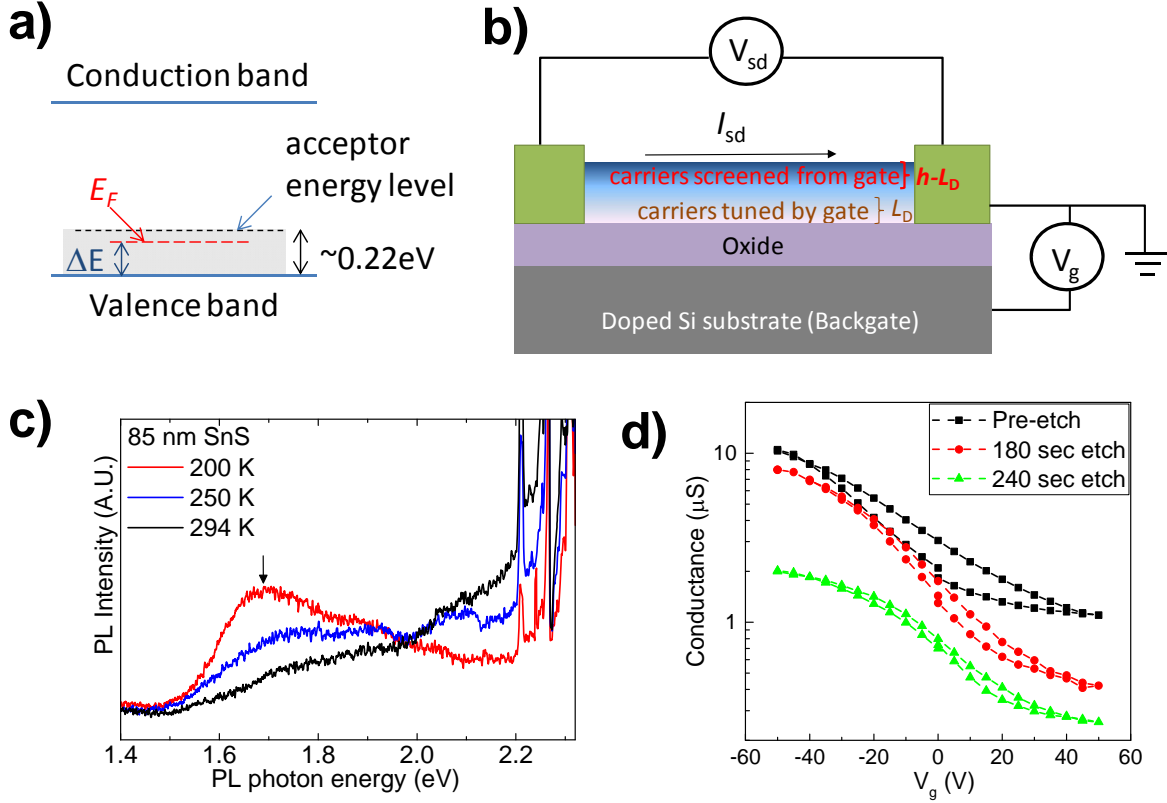


**Figure 4.** a) Schematic of relative positions of different energy levels. b) Schematic of carrier gating in multilayer SnS FET devices with thickness larger than the screening length  $L_D$ . Gate is only able to tune the bottom layer of the sample with the rest of sample unaffected by gate voltage. c) PL spectra at different temperatures of an 85-nm-thick SnS flake exfoliated onto Si/Si<sub>3</sub>N<sub>3</sub> substrate. The excitation photon energy is 2.33 eV. The superimposed sharp peaks above 2.2 eV are Raman lines from the sample or the substrate. d) Four-probe conductance *vs.*  $V_g$  of a SnS device upon plasma etching to thin the SnS flake.

Examining Eq.1, one sees that 2D semiconductor samples with heavier doping and larger thickness  $h$  are expected to have larger residual OFF-state conductance in the depletion regime and a poor ON-OFF ratio. SnS is known to be p-type due to rich intrinsic defects.<sup>22,23,28</sup> Photoluminescence (PL) measurements were performed to gain more insights on the impurity states. Figure 4c displays PL spectra from the 85 nm SnS sample at variable temperatures. A broad luminescence band centered at  $\sim 1.7$  eV becomes better defined when temperature is lowered and is clearly seen at 200 K. As noted in prior PL study on bulk SnS,<sup>34</sup> this PL band is likely from the radiative defect states, attesting the existence of rich defect states in SnS studied. Although fabricating SnS devices with thickness less than 50nm turned out to be difficult, we performed a study to investigate the SnS FET device's performance upon successive thinning of the sample by dry etching. As displayed in Figure 4d, after Ar ion etching at 300 W with Ar flow

of 30 sccm at 0.1 Torr for 180 sec, the OFF-state conductance was greatly suppressed and a higher ON-OFF ratio (red curve vs. black curve in Figure 4d) was obtained. Unfortunately, further ion etching over longer period of time likely created severe damage to the sample, resulting in sample's mobility being greatly reduced and the ON-OFF ratio cannot be further improved (green curve in Figure 4d).

We found that compensating the acceptors with n-type doping on the surface of SnS flake is an effective way to suppress the conductance of surface dead layer and improve the ON-OFF ratio of device. Previously,  $\text{Cs}_2\text{CO}_3$  was used to induce n-type doping in  $\text{MoS}_2$  and black phosphorus<sup>35,36</sup>. We compare the gate modulated conductance of a SnS device before and after evaporating 5 nm  $\text{Cs}_2\text{CO}_3$  on its surface. As demonstrated in Figure 5a, at least an order of magnitude increase in the ON-OFF ratio was achieved in the same device after surface n-type doping with  $\text{Cs}_2\text{CO}_3$ . Hall effect measurements showed that  $\text{Cs}_2\text{CO}_3$  doped sample has hole density about ten times lower than the pristine sample ( $10^{10}$ - $4 \times 10^{11}/\text{cm}^2$  at room temperature in Figure 5b vs.  $10^{11}$ - $10^{12}/\text{cm}^2$  in Figure 3a). The sample also demonstrated high hole mobility ( $\sim 100 \text{ cm}^2/\text{Vs}$  at room  $T$ ) comparable to the bulk value (Figure 5c). Note that the typical ON-OFF ratio of our SnS devices after n-type surface doping reached 100 but is significantly lower than that of TMD based (e.g.  $\text{MoS}_2$ ) FETs. We believe that more elaborated control of doping and using thinner SnS samples will further improve the switching performance of SnS based 2D FET devices.

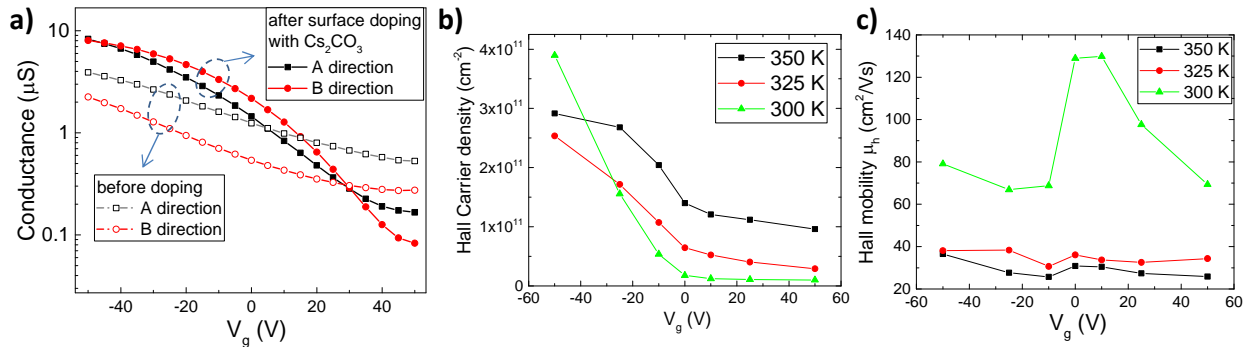


**Figure 5 a.) Comparison of 4-probe conductance vs. gate voltage at room temperature of SnS device between different direction and before and after doping with  $\text{Cs}_2\text{CO}_3$ . b.) Extracted Hall carrier density and d.) Hall mobility of the sample after doping with  $\text{Cs}_2\text{CO}_3$ .**

## CONCLUSION

In this work, p-type multilayer SnS FET devices were fabricated and studied. Thermally activated behavior in the temperature dependent conductance and Hall carrier density demonstrated that the holes in devices originate from acceptors with ionization energy  $\sim 0.22$  eV despite that no intentional doping was used in the SnS crystal. The devices showed good gate tunability in negative  $V_g$  towards accumulation yet the gate tuning effect was weak in positive  $V_g$  towards depletion. This contrast in the gate effect and the limited ON-OFF ratio could be attributed to the sample's thickness exceeding the maximum carrier screening length, allowing a residual conduction through a shunt layer near the top surface of sample. Through thinning the sample by etching or n-type surface doping, the device's ON-OFF ratio was improved by an order of magnitude. This work opens up routes towards high performance field effect devices based on IV-VI 2D mono-chalcogenides (SnS, SnSe *etc*) and points to the critical role of finite depletion depth in the switching performance (ON-OFF ratio, OFF-state conductance) of multilayer SnS devices. Since most 2D semiconductor FETs operate as depletion mode FET at room temperature, our findings here also offer insight to the understanding of other multilayer 2D semiconductor FETs. In particular, to obtain the best ON-OFF ratio, 2D semiconductor FETs should limit their thickness to within the Debye screening length (around 10 - 50 nm), beyond which there is a residual conductance from the top surface layer and a deteriorated ON-OFF ratio is expected. Similar conclusion regarding the deteriorated ON-OFF ratio with increasing thickness was reached in a recent study on multilayer MoS<sub>2</sub> FETs.<sup>37</sup>

## METHODS

**Bulk SnS Single Crystal.** SnS single crystals were prepared from the Sn and S 5N (99.999%) purity compounds. The synthesis of the compounds was carried out in conical quartz ampoules evacuated to  $10^{-4}$  Pa. The homogenization of the batches and synthesis of the compounds was carried out in a horizontal furnace at 900 °C for 48 h. The mixed crystals were grown by a vertical Bridgman method. Before pulling, the ampoules containing the melt were heat-treated at 900 °C for 24 h and when the melt filled the tip of ampoule, the ampoules were lowered through the temperature gradient at a rate of 0.1 mm/h. The amount of single crystalline areas was successfully increased by a reduction of the growth velocity from 5 mm/h to 0.5 mm/h. Approximately 2/3 of the whole sample volume is single crystalline, due to the still present stress

during the phase transition. The obtained SnS single crystals were 3 cm long and 1.2 cm in diameter. They exhibited good cleavability in the direction perpendicular to the trigonal axis  $c$ , i.e. along the (001) plane. This preparation gave homogeneous single crystals with well-developed cleavage faces. These faces, being perpendicular to the  $c$ -axis, were always parallel with the direction of pulling, i.e. with the ampoule axis. The crystal structure is shown in Figure 1a.

**Multilayer SnS Device Fabrication.** The bulk SnS was then exfoliated onto degenerately doped Si substrates with silicon oxide or silicon nitride on surface. Electron beam lithography process with standard PMMA/MMA copolymer bilayer resist and metal deposition of Ni were subsequently used to create contacts for four-probe electrical transport characterization, as demonstrated in Figure 1.  $b$ .  $A$  direction corresponds to  $Y$  axis while  $B$  direction corresponds to  $Z$  axis and  $X$  axis is the exfoliation direction. Sample is a single crystal flake as demonstrated by XRD result shown in Figure 3c, and the sample generally has thickness ranging from 40-120 nm.

**Electrical transport characterization.** Samples were measured in a Quantum Design PPMS (Physical Property Measurement System) or Lakeshore Cryogenic probe station. Hall measurements were conducted by varying magnetic field at various temperatures. For DC current-voltage characterization, a National Instrument PCI-6221 DAQ card integrated computer along with a BNC-2090 terminal block and a Stanford Research Systems SR-570 low noise current preamplifier were used to supply bias and measure current. A LabVIEW program was used to record data. For four-probe conductance and Hall resistance measurement, lockin technique was used where a 7 Hz sine wave voltage was applied to the sample. Current and four-probe voltage were measured by a SR-830 lockin amplifier.

**Raman and PL.** Raman and photoluminescence (PL) measurements were conducted using a Horiba Labram HR Raman microscope system. A 532 nm laser light was used. The laser was focused on sample surface using a 50 $\times$  objective lens (spot diameter of about 2  $\mu\text{m}$ ). Instrument resolution was 0.5  $\text{cm}^{-1}$  for Raman measurements and 2  $\text{cm}^{-1}$  for PL measurements. Samples were mounted in an optical cryostat for variable temperature measurements.

## ACKNOWLEDGEMENT

X.P.A.G. thanks the National Science Foundation (DMR-1151534) for its financial support and Jun Zhu for helpful discussions. Y.T.C. acknowledges the Ministry of Science and Technology of Taiwan (grant No. MOST-103-2627-M-002-009) for financial support. R.S. and F.C.C. acknowledge the support provided by the Academia Sinica research program on Nanoscience and Nanotechnology under project number NM004. Work at the University of Northern Iowa (UNI) is supported by the National Science Foundation (NSF, Grant No. DMR-1552482 (C.H.) and DMR-1410496 (R.H.)) and the ACS PRF grant (No. 53401-UNI10 (C.W.)). The low temperature equipment at UNI was acquired through the NSF MRI Grant (No. DMR-1337207). R. H. also acknowledges support by the UNI Faculty Summer Fellowship.

## REFERENCES

1. Novoselov, K.S.; Geim, A.K.; Morozov, S.V.; Jiang, D.; Katsnelson, M.I.; Grigorieva, I.V.; Dubonos, S.V.; Firsov. Two-dimensional gas of massless Dirac fermions in graphene. *Nature* **2005**, 438, 197–200.
2. Zhang, Y.; Tan, Y.-W.; Stormer, H. L.; Kim, P. Experimental observation of the quantum Hall effect and Berry's phase in graphene. *Nature* **2005**, 438, 201–204.
3. Wang, Q.H.; Kalantar-Zadeh, K.; Kis, A.; Coleman, J.N.; Strano, M.S. Electronics and optoelectronics of two-dimensional transition metal dichalcogenides. *Nat. Nano.* **2012**, 7, 699–712.
4. Geim, A. K.; Grigorieva, I. V. Van der Waals heterostructures. *Nature* **2013**, 499, 419–425.
5. Chhowalla, M.; Shin, H.S.; Eda, G.; Li, L.-J.; Loh, K.P.; Zhang, H.; The chemistry of two-dimensional layered transition metal dichalcogenide nanosheets. *Nat. Chem.* **2013**, 5, 263–275.
6. Duan, X.; Wang, C.; Pan, A.; Yu, R.; Duan, X. Two-dimensional transition metal dichalcogenides as atomically thin semiconductors: opportunities and challenges. *Chem. Soc. Rev.* **2015**, 44, 8859–8876 (2015).

7. Mak, K. F.; Shan, J. Photonics and optoelectronics of 2D semiconductor transition metal dichalcogenides. *Nat. Photon.* **2016**, 10, 216–226.
8. Radisavljevic, B.; Radenovic, A.; Brivio, J.; Giacometti, V.; Kis, A. Single-layer MoS<sub>2</sub> transistors. *Nat. Nano.* **2011**, 6, 147–150.
9. Ghatak, S.; Pal, A. N.; Ghosh, A. Nature of Electronic States in Atomically Thin MoS<sub>2</sub> Field-Effect Transistors. *ACS Nano* **2011**, 5, 7707–7712.
10. Fuhrer, M. S.; Hone, J. Measurement of mobility in dual-gated MoS<sub>2</sub> transistors. *Nat. Nano.* **2013**, 8, 146–147 (2013).
11. Larentis, S.; Fallahazad, B.; Tutuc, E. Field-effect transistors and intrinsic mobility in ultra-thin MoSe<sub>2</sub> layers. *Appl. Phys. Lett.* **2012**, 101, 223104.
12. Das, S.R.; Kwon, J.; Prakash, A.; Delker, C.J.; Das, S.; Janes, D.B. Low-frequency noise in MoSe<sub>2</sub> field effect transistors. *Appl. Phys. Lett.* **2015**, 106, 83507.
13. Hwang, W.S.; Remskar, M.; Yan, R.; Protasenko, V.; Tahy, K.; Chae, S.D.; Zhao, P.; Konar, A.; Xing, H. (Grace), Seabaugh, A.; Jena, D. Transistors with chemically synthesized layered semiconductor WS<sub>2</sub> exhibiting 10<sup>5</sup> room temperature modulation and ambipolar behavior. *Appl. Phys. Lett.* **2012**, 101, 13107.
14. Iqbal, M.W.; Iqbal, M.Z.; Khan, M.F.; Shehzad, M.A.; Seo, Y.; Park, J.H.; Hwang, C.; Eom, J. High-mobility and air-stable single-layer WS<sub>2</sub> field-effect transistors sandwiched between chemical vapor deposition-grown hexagonal BN films. *Sci. Rep.* **2015**, 5, 10699.
15. Pradhan, N. R. *et al.* Hall and field-effect mobilities in few layered p-WSe<sub>2</sub> field-effect transistors. *Sci. Rep.* **2015**, 5, 8979.
16. Liu, H.; Chen, J.; Yu, H.; Yang, F.; Jiao, L.; Liu, G.-B.; Ho, W.; Gao, C.; Jia, J.; Yao, W.; Xie, M. Observation of intervalley quantum interference in epitaxial monolayer tungsten diselenide. *Nat. Comm.* **2015**, 6, 8180.

17. Li, L.; Yu, Y.; Ye, G.J.; Ge, Q.; Ou, X.; Wu, H.; Feng, D.; Chen, X.H.; Zhang, Y. Black phosphorus field-effect transistors. *Nat. Nano.* **2014**, *9*, 372–377.
18. Liu, H.; Neal, A.; Zhu, Z.; Luo, Z.; Xu, X.; Tomanek, D.; And Ye, P. Phosphorene: An Unexplored 2D Semiconductor with a High Hole Mobility. *ACS Nano*, **2014**, *8* (4), 4033-40471.
19. Sucharitakul, S.; Goble, N.J.; Kumar, U.R.; Sankar, R.; Bogorad, Z.A.; Chou, F.-C.; Chen, Y.-T.; Gao, X.P.A. Intrinsic Electron Mobility Exceeding  $10^3$  cm<sup>2</sup>/(V s) in Multilayer InSe FETs. *Nano Lett.* **2015**, *15*, 3815–3819.
20. Tamalampudi, S. R. *et al.*, High Performance and Bendable Few-Layered InSe Photodetectors with Broad Spectral Response. *Nano Lett.* **2014**, *14*, 2800–2806.
21. Chuang, H.; Chamlagain, B.; Koehler, M.; Perera, M.; Yan, J.; Madrus, D.; Tomanek, D. and Zhou, Z. Low-Resistance 2D/2D Ohmic Contacts: A Universal Approach to High-Performance WSe<sub>2</sub>, MoS<sub>2</sub>, and MoSe<sub>2</sub> Transistors, *Nano Lett.* **2016**, *16* (3), 1896–1902.
22. Ran, F.-Y.; Xiao, Z.; Hiramatsu, H.; Hosono, H.; Kamiya, T. Growth of high-quality SnS epitaxial films by H<sub>2</sub>S flow pulsed laser deposition. *Appl. Phys. Lett.* **2014**, *104*, 72106.
23. Ran, F.-Y.; Xiao, Z.; Toda, Y.; Hiramatsu, H.; Hosono, H.; Kamiya, T. n-type conversion of SnS by isovalent ion substitution: Geometrical doping as a new doping route. *Sci. Rep.* **2015**, *5*, 10428.
24. Zhao, L.-D.; Lo, S.-H.; Zhang, Y.; Sun, H.; Tan, G.; Uher, C.; Wolverton, C.; Dravid, V.P.; Kanatzidis, M.G. Ultralow thermal conductivity and high thermoelectric figure of merit in SnSe crystals. *Nature* **2014**, *508*, 373–377.
25. Shi, G.; Kioupakis, E. Quasiparticle band structures and thermoelectric transport properties of p-type SnSe. *J. of Appl. Phys.* **2015**, *117*, 65103.

26. Guo, R.; Wang, X.; Kuang, Y.; Huang, B. First-principles study of anisotropic thermoelectric transport properties of IV-VI semiconductor compounds SnSe and SnS. *Phys. Rev. B* **2015**, *92*, 115202.
27. Zhao, S.; Wang, H.; Zhou, Y.; Liao, L.; Jiang, Y.; Yang, X.; Chen, G.; Lin, M.; Wang, Y.; Peng, H.; Liu, Z. Controlled synthesis of single-crystal SnSe nanoplates. *Nano Res.* **2015**, *8*, 288–295.
28. Albers, W.; Haas, C.; Vink, H. J. and Wasscher, J. D. Investigations on SnS. *J. Appl. Phys.* **1961**, *32*, 2220.
29. Rodin, A. S.; Gomes, L. C.; Carvalho, A.; Castro Neto, A. H. Valley physics in tin (II) sulfide. *Phys. Rev. B* **2016**, *93*, 45431.
30. Chandrasekhar, H. R.; Humphreys, R. G.; Zwick, U.; Cardona, M. Infrared and Raman spectra of the IV-VI compounds SnS and SnSe. *Phys. Rev. B* **1977**, *15*, 2177–2183.
31. Raadik, T.; Grossberg, M.; Raudoja, J.; Traksmaa, R.; Krustok, J. Temperature-dependent photoreflectance of SnS crystals. *J. of Phys. and Chem. of Sol.* **2013**, *74*, 1683–1685 (2013).
32. Dayeh, S.A.; Aplin, D.P.R.; Zhou, X.; Yu, P.K.L.; Yu, E.T.; Wang, D. High Electron Mobility InAs Nanowire Field-Effect Transistors. *Small* **2007**, *3*, 326–332.
33. Simon M. S.; Kwok K. Ng. *Physics of Semiconductor Devices*, **2007**, 3rd Edition, Wiley.
34. Devika, M.; Koteeswara Reddy, N.; Prashantha, M.; Ramesh, K.; Venkatramana Reddy, S.; Hahn, Y.B.; Gunasekhar, K.R. The physical properties of SnS films grown on lattice-matched and amorphous substrates. *Phys. Stat. Sol. (a)* **2010**, *207*, 1864–1869.
35. Lin, J.; Han, Ch.; Wang, F.; Wang, R.; Xiang, D. Qin, Sh.; Zhang, X.; Wang, L.; Zhang, H.; Wee, A. and Chen, W. Electron-Doping-Enhanced Trion Formation in Monolayer Molybdenum Disulfide Functionalized with Cesium Carbonate, *ACS Nano*, **2014**, *8* (5), 5323–5329.

36. Xiang, D.; Han, C.; Wu, J.; Zhong, S.; Liu, Y.; Lin, J.; Zhang, X.-A.; Ping Hu, W.; Özyilmaz, B.; Neto, A.H.C.; Wee, A.T.S.; Chen, W. Surface transfer doping induced effective modulation on ambipolar characteristics of few-layer black phosphorus. *Nat. Comm.* **2015**, 6, 6485.
37. Zhang, Y.; Li, H.; Wang, H.; Xie, H.; Liu, R.; Zhang, S.-L.; Qiu, Z.-J. Thickness Considerations of Two-Dimensional Layered Semiconductors for Transistor Applications. *Sci. Rep.* **2016**, 6, 29615.

TOC Figure

